Deployment Strategies for Representative Surveys using Passive Drifting Seafloor Imaging Floats

Qiuchang Yang, Miquel Massot-Campos, Subhra K. Das, Blair Thornton*
Centre for In Situ and Remote Intelligent Sensing,
Faculty of Engineering and Physical Science
University of Southampton, Southampton, United Kingdom
*Institute of Industrial Science, The University of Tokyo, Tokyo, Japan
qy1n19, miquel.massot-campos, subhra_k.das, b.thornton@soton.ac.uk

Oscar Pizarro
Australian Centre for Field Robotics
University of Sydney
Sydney, Australia
o.pizarro@acfr.usyd.edu.au

***Abstract*—This paper develops a method to simulate the trajectories of Lagrangian imaging floats and evaluate the effectiveness of different deployment strategies when planning sparse sampling surveys of seafloor regions in the order of 1-25 km^2 over periods of several weeks or months. The method combines time-varying current depth profiles with bathymetry to simulate the drift trajectories of platforms that keep a constant altitude off the seafloor. To achieve better targeting of observations, time-reverse simulations are used to determine surface deployment locations that are predicted to pass through specific points on the seafloor. The reward function used to evaluate each deployment plan considers both the total area and distribution of the predicted observations in a region of interest. We assess different observation strategies, comparing stratified and randomised distributions, and investigating the impact of different dive durations, numbers of platforms and seasonal sensitivity on the reward score for four real-world deployment scenarios. The results show that for a given survey duration there exists an optimum dive duration for different depths and sizes of region for efficient representation, and that the sensitivity of the reward to operational choices is higher for smaller survey regions.**

I. Introduction

Robotic seafloor imaging is becoming increasingly recognised as a necessary component of environmental baseline and infrastructure impact assessment surveys [1]. The strong attenuation of light in water means that the areas that can be imaged are typically limited to $\sim$1,000 m^2/h, where the platforms used need to provide their own illumination and operate within a few metres of the seabed. The low cover rates are compounded by the high cost and limited endurance of the autonomous underwater vehicles (AUVs) typically used to perform imaging surveys, and this motivates research into alternative, low-cost approaches to seafloor imaging.

Lagrangian imaging floats [2] have lower unit and operational costs than AUVs. They are equipped with cameras, strobes and vertical thrusters to keep a constant altitude while they gather imagery, and do not require expensive navigational sensors since they do not control their location in real time. Imaging floats are energetically efficient as they do not propel themselves laterally, instead drifting passively on currents near the seafloor. Actuators are only used to dive and maintain a constant altitude during their observations. If mission endurances of several weeks or months can be achieved, the reliance on crewed vessels with expert operators and facilities for energy replenishment can be reduced, making these platforms suitable for deployment in large numbers. Although precisely targeted or structured observations (e.g. dense/sparse grids, depth transects, contour following) cannot be achieved, for application where large regions of the seafloor are only sparsely observed (e.g. environmental baseline and impact monitoring) the lower cost per observation, increased area cover and reduced need for operational expertise make Lagrangian floats an attractive option for region-scale imaging surveys.

Although not all applications require metre precise targeting of seafloor locations to observe, most benefit from the ability to loosely target regions and structure observations for effective representation. This research develops a method to plan and assess different deployment strategies for efficient sampling of large seafloor regions using imaging floats. The method uses seafloor current predictions and bathymetric models to simulate drift trajectories at low altitudes, introducing time-reverse simulations for better targeting of observations and a reward function to better understand the impacts of operational choices. The platforms targeted in this work are the DriftCam imaging floats being developed at the University of Southampton [3]. These can be programmed to surface after any interval up to their design endurance of two weeks, and can be recovered, relocated and redeployed by simple support boats during their energy cycle to achieve more widely distributed observations. Since the platforms do not require energy replenishment or re-tasking during this phase, these operations can be performed by non-experts and could potentially be automated.

II. Literature review

There are several constraints that need to be considered when planning marine surveys. The target region of interest and time of year a survey takes place is often determined by factors outside a platform operator's control. The survey duration and number of platforms used are also typically limited by resource availability. However, there are several choices such as deployment location and dive duration that are more flexible and can impact the quality of observations

that are achieved. For sparse surveys, planning deployments becomes a compressive sensing challenge where the aim is to reconstruct information about regions using a small number of observations by making assumption about the spatial distribution of features of interest [4]. Sparse sub-sampling methods are widely used in medical imaging, communications and mapping applications [5], where most applications favour randomised point sampling as the observations can describe patterns that exist on different temporal or spatial frequencies. However, in mobile mapping applications observations are made continuously along the trajectory of a platform, and there is a large cost associated with platform recovery and redeployment needed to approach random point observations. There are examples where observations are performed along randomised line trajectories to sample a large range of spatial frequencies along different directions. In practise however, many environmental survey applications favour spatially stratified approaches that span the full extent of a region of interest. This allows for balanced treatment of observation units to capture trends spanning the region of interest [6], and is useful for change detection as it allows for more consistent representation between survey efforts [7].

Targeted observation locations can be spatially stratified or randomised to varying degrees, where for drifting platforms, the duration of each drift can be reduced to allow for more widely distributed, point-like sampling, or extended to make observations along continuous trajectories. Although in many mobile mapping applications the heading of trajectories themselves can be purposely randomised or structured, for Lagrangian floats the trajectories are prone to being similar over multi-kilometre scales during a given time window due to the currents that drive them. Examples of drift based marine surveys include the Argo project, where equal interval spatial sampling approaches are targeted for large scale distributed sampling at a global scale [8]. Drifting platforms have also been used for surveys at smaller scales, where Salman et al., 2008 [9] investigated optimal drifter deployments to characterise local flow fields, and Johanna et al., 2018 presented an optimised deployment planning method that simultaneously models and exploits an unknown flow field in a $5\,\mathrm{km}^2$ region [10] for surface drifter augmented Autonomous Surface Vehicle (ASV) surveys. To date however, studies of drifter deployment methods have targeted flow field characterisation or measurement of physical and chemical properties of the water-column, whereas methods to understand the sensitivity of seafloor surveys to different deployment strategies and conditions have not been investigated.

III. Method

To understand the success and sensitivity of different imaging float deployment strategies to operational choices, it is necessary to simulate the trajectories of constant altitude keeping platforms and develop a set of criteria for their evaluation. Fig.1 gives an overview of the method developed in this work. The inputs to the framework consist of the survey region, defined by the bounding coordinates of the region of interest,

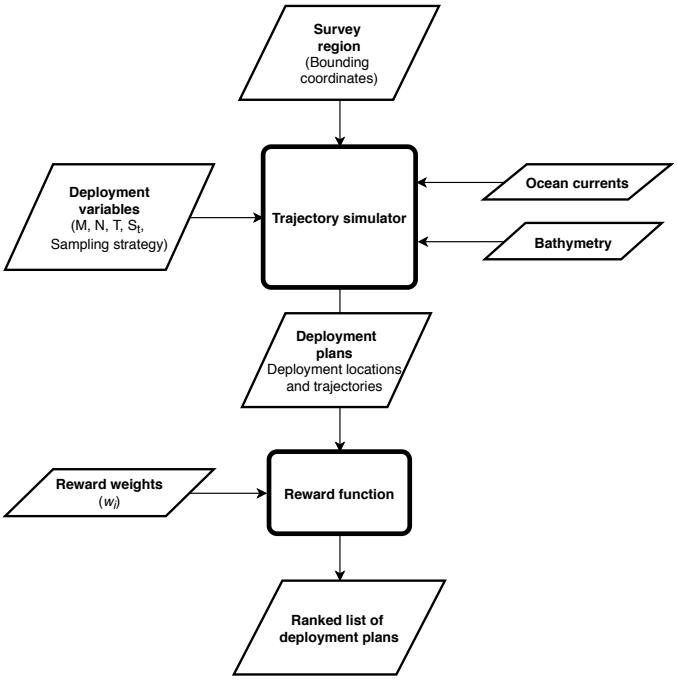

Fig. 1: Overview of the deployment planner

deployment variables and reward weights. The deployment variables considered here include the number of deployments per drifter, M, number of drifters, N, total survey duration, T, start date and time of the survey, $\mathrm{S_t}$, and the sampling strategy. The weighted reward function used to evaluate the deplyoment plans is described in section III-B. Once these variables are defined, the trajectory simulator uses available time-varying current profiles and bathymetry data to generate a set of deployment plans, which are then evaluated by the reward function to rank the deployment plans.

A. Trajectory simulation

The trajectory simulator developed here modifies the *Parcels* particle trajectory modelling framework developed to simulate the trajectories of Argo floats used in physical oceanography [11]. It provides a set of equations to calculate particle trajectories through four dimensional gridded space, (x, y, z, t), where x, y, z are Cartesian coordinates and t is time,

$$X(t + \delta t) = X(t) + \int \overrightarrow{V}\,\delta t, \tag{1}$$

$\overrightarrow{V} = u, v, w$ denotes the flow field and is a function of location and time $\overrightarrow{V} = \overrightarrow{V}(x, y, z, t)$, and $X(t)$ denotes the position of a particle at time t. Since the drifters considered in this work have vertical actuation, equation (1) is only used to calculate the position of the drifters in the lateral direction. During seafloor observation the platform's depth, z, is determined as,

$$z = D(x, y) + h \tag{2}$$

where $D(x, y)$ is the depth of the seafloor at the platform's location, and h is the target altitude. During diving and

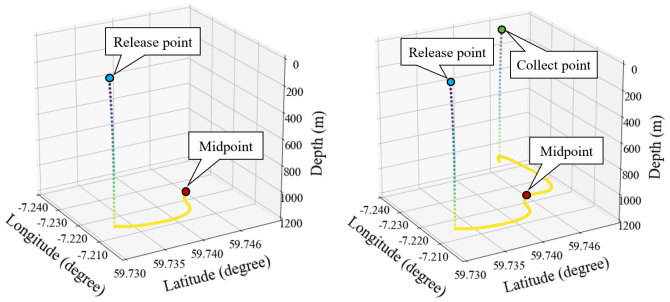

(a) Time-reverse simulation (b) Forward simulation

Fig. 2: Time-reverse and time forward simulations used to generate deployment locations and trajectories passing through target seafloor locations.

surfacing, we assume a constant vertical speed based on the target platform's specification. The time varying flow fields used in equation (1) and the bathymetry data used in equation (2) can be obtained from Ocean General Circulation Models (OGCM) and global bathymetry repositories.

To generate trajectories that pass through specific target locations on the seafloor, the simulator uses time-reverse simulations. These start with a desired target location to observe for each drift, which is determined using the deployment variables M, N and a sampling strategy. Defining how long into each drift the target location should be observed allows the simulator to determine the deployment location by using equations (1) and (2) with time decreasing for the defined period, taking into account the time needed for the platform to dive from the surface. Fig. 2a shows this where the target location is observed at the midpoint of the dive. After this, a forward simulation finds the surfacing location by simulating the remaining drifting time, taking into account the time needed to surface from its final observation as shown in Fig. 2b.

B. Reward function

For platforms that make continuous observations along current driven trajectories, the target region will be densely sampled along track and sparsely across the currents, introducing potential bias in any subsequent analysis. To address this problem, platforms can be set to have a short dive duration and be redeployed to achieve more spatially stratified or randomised observations. However, redeployment of seafloor mapping platforms reduces the total observation area since the time spent on surfacing, recovery, relocation, redeployment and diving does not yield useful data.

To understand these and other impacts of operational choices on a survey, we define a reward function that considers the total area observed within the survey region of interest and the spatial distribution of observations as follows,

$$R = \sum_{i=1}^{4} w_i \times r_i, \tag{3}$$

TABLE I: Components of the reward function

Index (i)	Description
1	Total area observed
2	Spatial distribution of observations
3	Distance from edges of the region
4	Proportion of time in the target region

where r_i is a non-dimensional component of the reward, w_i is the user defined weight where $\sum_i w_i = 1$, and i denotes the index for each reward component as defined in table I. Our target region is represented by a $m \times n$ grid bounded by C_{DL} and C_{UR}. P as a 2D list of all trajectory points simulated.

The reward component r_1 is defined as

$$r_1 = \frac{\sum_{j=1}^{m} \sum_{k=1}^{n} cell(j,k)}{m \times n}, \tag{4}$$

$$cell(j,k) = 1, \ \ \forall \ \ P^* \ \ \text{where} \ \ P^* = P \in [C_{DL}, C_{UR}], \tag{5}$$

The distribution of observations, r_2 is defined as

$$r_2 = \sqrt{\frac{\sum_{i \neq j} |P_i^* - P_j^*\|^2}{L(L-1)}} \tag{6}$$

where, $L = |P^*|$. The reward component for distance from the edges of the region bounding box r_3 is introduced to prevent observations being concentrated at the extremities, and is defined as

$$r_3 = \frac{1}{0.5 \times \max(A,B)} \sqrt{\frac{\sum^{L} e(P^*)^2}{L}}, \tag{7}$$

where, $A \times B$ is the region area and

$$e(P^*) = \min |P^* - (C_{DL}, C_{UR})|. \tag{8}$$

The reward score for time proportion, r_4, is defined as,

$$r_4 = \frac{L \times dt}{N \times \mathrm{T}} \tag{9}$$

where dt is the simulation time step.

Fig. 3 illustrates the behaviour of the reward function for simple observation configurations. The top row outscores the bottom as it covers a larger area. The centre column outscores the left column because the observations are further from the edge of the bounding box, and the right column outscores the other columns as the observations are more evenly distributed. The sensitivity of the scores reflects the choice of reward weightings used, and these can be adapted based on the requirements of the survey.

IV. Experiments

We evaluate four scenarios shown in table II for the locations in Fig. 5. Scenario A targets a $1\,\mathrm{km}^2$ region on the Tautra ridge in Trondheim, Norway, a tide-dominated shallow Fjord. Scenario B targets a $5\,\mathrm{km}^2$ region in Plocan, off the Canary Islands, which represents a sheltered shallow region in the Atlantic. Scenarios C and D target $1\,\mathrm{km}^2$ and $5\,\mathrm{km}^2$ regions respectively in the Darwin mounds, a deep-water marine protected area in the North Atlantic.

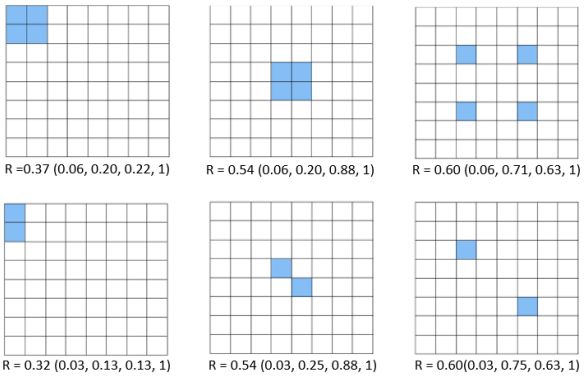

Fig. 3: Simple observation scenarios and reward scores for $w = [1/4, 1/4, 1/4, 1/4]$. Blue cells indicate observations, and the brackets show the reward components r_i.

We investigate the impact of different sampling strategies, values for deployment variables M and N and seasonal variations in the currents on the reward scores. For the present paper we study two sampling strategies, one consisting of fully randomised drift midpoints within the survey area, and the other where midpoints are loosely stratified using the Poisson disc algorithm, illustrated in Fig. 4.

The survey duration is fixed to T = 10 days with flow field data starting from S_t = 12:00 UTC, 5^{th} April 2020. M varies from 1 to 100 (i.e. deployment periods of 10 days to 2.4 h) and N varies from 1 to 5. Diving and surfacing rates of 1.0 m/s are used where the recovery, relocation and redeployment period is set to 1 hour, which is reasonable considering size of the survey regions, number of platforms and the fact that energy replenishment of the platforms is not necessary. The drifting altitude is set to 2 m off the seafloor and the reward is calculated for a target region cell size of 50 m×50 m. The flow fields and bathymetry are obtained from Copernicus (https://marine.copernicus.eu/) and GEBCO gridded bathymetric (https://www.gebco.net/) repositories. The flow fields have $1/12$ degree longitude and latitude resolution, with depth profiles consisting of 50 levels over the depth range at each lateral location, with a temporal resolution of one day. GEBCO's gridded bathymetric data has a resolution of ∼460 m at the equator. Although higher resolution data is available, the advantage of these repositories is that data is available for any point on the seafloor.

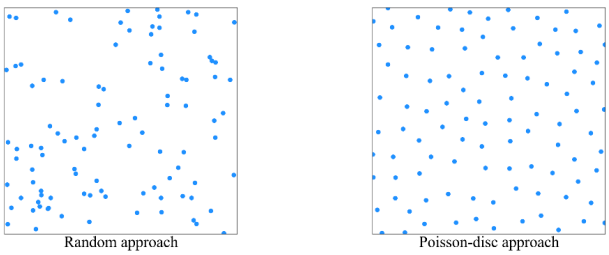

Fig. 4: Different sampling strategies adopted in this work.

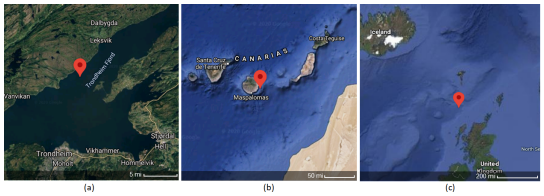

Fig. 5: Google earth images of the survey regions: (a) Tautra, Trondheim Fjord, (b) Plocan, (c) Darwin mounds

TABLE II: Operating scenarios.

Scenario	Center of region	Area (km^2)	Depth (m)
A	(63.595^0 N, 10.517^0 E)	1×1	0-200
B	(27.871^0 N, 15.340^0 W)	5×5	0-200
C	(59.758^0 N, 7.216^0 W)	1×1	1000-1500
D	(59.758^0 N, 7.216^0 W)	5×5	1000-1500

V. Results

To understand behavior of variables M and N, we first perform experiments with fixed values of T and S_t. Next we investigate the robustness of the reward scores achieved for fixed vales of M and N, where S_t varies over a year. Fig. 6 shows the scores for all scenarios with M and N varying. The results show that there exists an optimal dive duration (i.e. M). For small M values, the scores initially increase as the long trajectories have a large component outside of the region of interest and have a poor distribution (see Fig. 7c). As M increases, the transects are shorter with a larger proportion of observations made in the target region, and have a more even distribution (see Fig. 7d). However, after a certain point, the period of non-observation due to the redeployment cycle reduces the total area observed in the survey area, resulting in a peak M value. Table III shows that the optimum M values are higher in Scenarios A and B, corresponding to shallow regions, than in the deeper Scenarios C and D. This is to be expected as the diving and surfacing transit time is larger. Increasing the number of platforms always increases the score, which is expected as a larger area gets observed. Comparing Scenarios A and C with B and D, the peak M value is larger for smaller regions (A and C) than the larger regions (B and D) with similar depths. We also see that the scores are more sensitive to the deployment variables in smaller survey regions. This is because the gains in observed area, r_1 (see eqn. (4)), have a larger relative contribution to the final reward. We also see that the Poisson-disc method outperforms the random method in these scenarios, but has marginally lower scores for scenarios B and D. This is because Poisson-disc ensures the corners and edges of the survey region are observed, as seen in Fig. 7a and b. In this example, the deployment duration is short and the observed regions remain mostly in the target region of interest, but for smaller values of M (i.e. longer dive times), trajectories near the edges are prone to drift outside of the region of interest, reducing both the coverage (r_1) and time proportion (r_4) reward components.

The peak M values and preferred deployment strategies

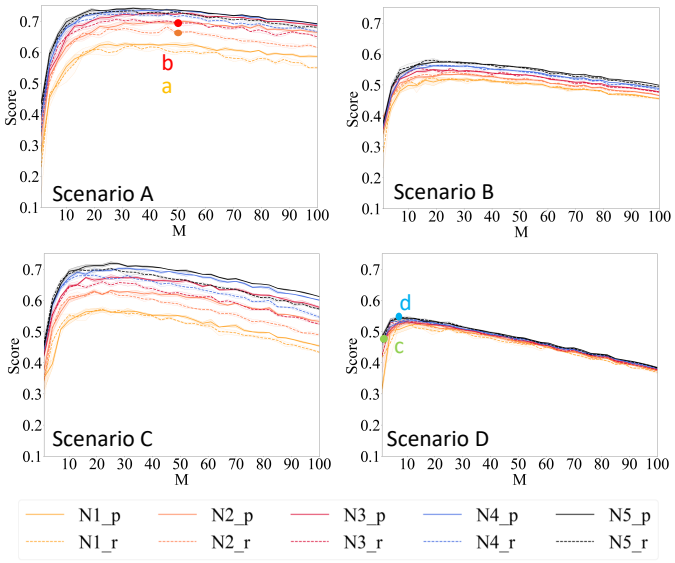

Fig. 6: Scores for $w = [1/4, 1/4, 1/4, 1/4]$ for [M,N,T]=[1-100,1-5,10]. The markers and labels correspond to Fig. 7

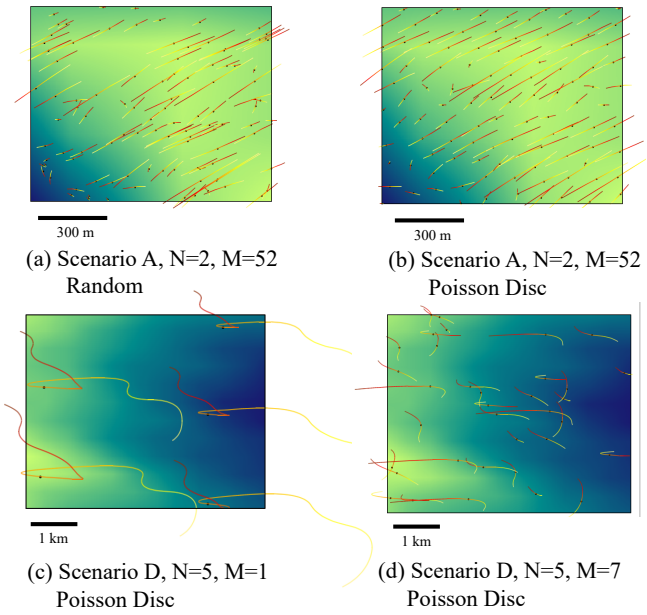

(a) Scenario A, N=2, M=52 Random

(b) Scenario A, N=2, M=52 Poisson Disc

(c) Scenario D, N=5, M=1 Poisson Disc

(d) Scenario D, N=5, M=7 Poisson Disc

Fig. 7: Trajectories for different scenarios and deployment variables correspond to the markers in Fig. 6.

TABLE III: Peak M values for the scenarios in Fig. 6. The summary shows the mean and standard deviation of the peak M values for all N and their respective scenario scores.

Scenarios		Poisson-disc method					Random method					Summary (N= 1-5)	
		N=1	N=2	N=3	N=4	N=5	N=1	N=2	N=3	N=4	N=5	mean	std
A	M	31	52	52	46	**34**	34	46	28	31	34	39	9
	Score	0.63	0.70	0.73	0.74	**0.74**	0.62	0.68	0.71	0.72	0.73	0.70	0.04
B	M	31	40	37	31	31	37	25	25	34	**19**	31	6
	Score	0.53	0.56	0.57	0.59	0.60	0.53	0.56	0.58	0.59	**0.60**	0.57	0.02
C	M	22	25	25	31	**25**	22	19	22	19	25	24	4
	Score	0.57	0.63	0.68	0.70	**0.72**	0.57	0.63	0.66	0.68	0.70	0.65	0.05
D	M	13	10	10	13	10	10	10	13	10	**7**	11	2
	Score	0.52	0.53	0.53	0.53	0.54	0.53	0.54	0.53	0.54	**0.55**	0.53	0.01

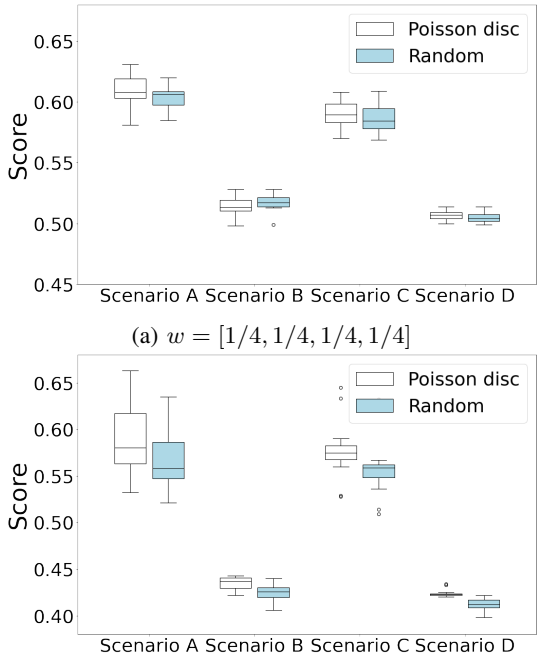

(a) $w = [1/4, 1/4, 1/4, 1/4]$

(b) $w = [1/3, 1/3, 1/3, 0]$

Fig. 8: Scores for Poisson-disc and random sampling with M=25, N=1, T=10, and S_t varying between 12:00 UTC, 5^{th} January 2019 and 12:00 UTC, 5^{th} December 2019.

depend on the chosen reward weights. Fig. 8 shows the scores for deployment plans with fixed values of M=25, N=1 and T=10, with varying deployment period start date. The scores for weights $w = [1/4, 1/4, 1/4, 1/4]$ (Fig. 8a) show that for larger regions (Scenarios B and D) the random sampling strategy outscores the Poisson-disc, as w_4 penalises the time spent outside of the target region by drifters deployed near the edges of the survey area. Although this is appropriate when operating near exclusion zones or busy shipping lanes, there are also situations where a platform drifting outside the target region is not a problem. In these situations, the distribution of observations within the target region should be prioritised, which can be achieved by reducing w_4. Fig. 8b shows the rewards for $w = [1/3, 1/3, 1/3, 0]$, where the Poisson-disc outscores random distribution in all scenarios, reflecting a more favourable distribution of observations in the survey area.

Figure 9 shows the variation of scores for $w = [1/3, 1/3, 1/3, 0]$ with S_t varying over a year at a resolution of 1 month. The plot shows the average of three simulations run under each condition and their standard deviations. The difference in scores reflects the seasonal changes in currents, which results in a variation of 1-7% for the different scenarios. Smaller regions are more sensitive to these effects, and in all cases, the effects are smaller than the impact achieved by varying M and N over the ranges studied in this work. There is no significant difference of the seasonal impact on the Poisson-disc and random approaches, but for the weights used here, the Poisson-disc always outscores the random approach.

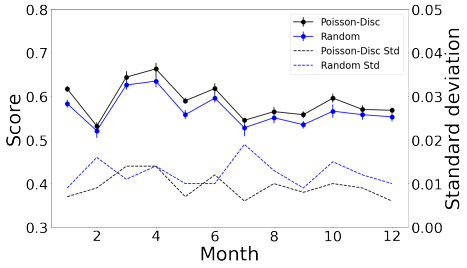

(a) Scenario A

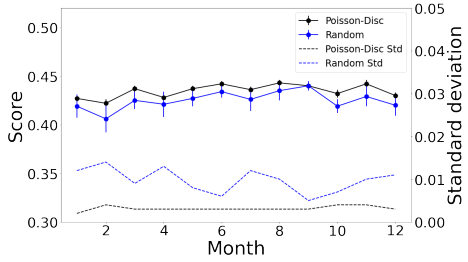

(b) Scenario B

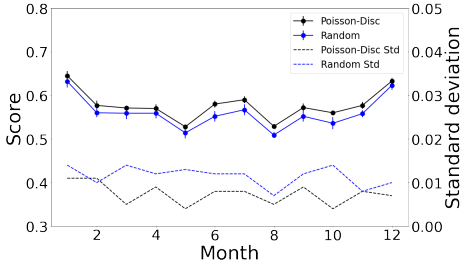

(c) Scenario C

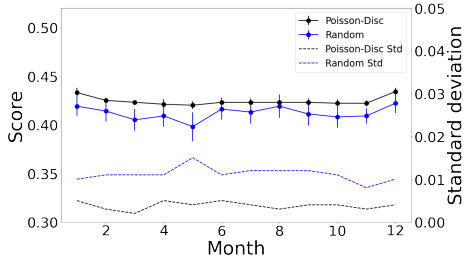

(d) Scenario D

Fig. 9: Scores for $w = [1/3, 1/3, 1/3, 0]$ where [M,N,T]=[25,1,10] for different deplyment periods in 2019.

VI. Conclusion

We have developed a method to plan region-scale deployments of passive drifting seafloor imaging floats. We studied the success and sensitivity of different deployment variables on the distribution and cover of observations for four deployment scenarios. This showed that for a given survey duration, an optimal number of deployments per platform (i.e dive duration) exists, and this depends on the size and depth of the survey region. The optimum is determined by a trade-off between the area covered within a survey region and the distribution of observations. For the region sizes considered, the reward score initially increases with the number of deployments per platform, and reduces after a point due to the time taken for redeployment when no observations are made. The rewards for smaller survey regions are more sensitive to operation choices, and the influence of seasonal variations in currents are smaller than the impact of the number of drifter units and their dive duration. The results show when the area and distribution of observations are prioritised, the Poisson-disc reliably outperforms random sampling, but carries an increased risk of platforms drifting outside the survey area.

A number of simplifications currently made require further investigation. The deployment duration here is uniform for all in a scenario, but units near downstream region edges would benefit from having shorter deployments to reduce the time spent outside of the survey area. The sensitivity to M also indicates more accurate modelling of the redeployment cycle time will be valuable. For deployment strategies, methods to optimise the target locations based on current profiles during each observation time window should be investigated to generate more dense and evenly distributed observations normal to the currents. Finally, the influence of current and bathymetry resolution should be investigated.

Acknowledgements

This work is funded by the UKRI EPSRC grant EP/S001182/1 and uses E.U. Copernicus Marine Service Information and the GEBCO Compilation Group 2019 Grid.

References

[1] T. Yamada, A. Prügel-Bennett, and B. Thornton, "Learning features from georeferenced seafloor imagery with location guided autoencoders," *Journal of Field Robotics*, vol. n/a, no. n/a. [Online]. Available: https://onlinelibrary.wiley.com/doi/abs/10.1002/rob.21961

[2] C. Roman, G. Inglis, and B. McGilvray, "Lagrangian floats as sea floor imaging platforms," *Continental Shelf Research*, vol. 31, no. 15, pp. 1592–1598, 2011.

[3] J. Cappelletto, M. Massot-Campos, A. Bodenmann, S. K. Das, and B. Thornton, "Micro-ballast dispenser for long endurance underwater mapping platforms," in *IEEE Underwater Technology Symp.*, 2019.

[4] D. L. Donoho, "Compressed sensing," *IEEE Transactions on Information Theory*, vol. 52, no. 4, pp. 1289–1306, 2006.

[5] Y. Mostofi, "Compressive cooperative sensing and mapping in mobile networks," *IEEE Transactions on Mobile Computing*, vol. 10, no. 12, pp. 1769–1784, 2011.

[6] J. Zhang and C. Zhang, "Sampling and sampling strategies for environmental analysis," *Intern. J. Environm. Anal. Chem*, vol. 92, no. 4, pp. 466–478, 2012.

[7] T. McDonald, "Review of environmental monitoring methods: Survey designs," *Environmental Monitoring and Assessment*, vol. 85, pp. 277–292, 2003.

[8] D. Roemmich, G. C. Johnson, S. Riser, R. Davis, J. Gilson, W. B. Owens, S. L. Garzoli, C. Schmid, and M. Ignaszewski, "The argo program: Observing the global ocean with profiling floats," *Oceanography*, vol. 22, no. 2, pp. 34–43, 2009.

[9] H. Salman, K. Ide, and C. K. R. T. Jones, "Using flow geometry for drifter deployment in lagrangian data assimilation," *Tellus A: Dynamic Meteorology and Oceanography*, vol. 60, no. 2, pp. 321–335, 2008. [Online]. Available: https://doi.org/10.1111/j.1600-0870.2007.00292.x

[10] J. Hansen and G. Dudek, "Coverage optimization with non-actuated, floating mobile sensors using iterative trajectory planning in marine flow fields," in *2018 IEEE/RSJ International Conference on Intelligent Robots and Systems (IROS)*, 2018, pp. 1906–1912.

[11] P. Delandmeter and E. Van Sebille, "The parcels v2. 0 lagrangian framework: new field interpolation schemes," *Geoscientific Model Development*, vol. 12, no. 8, pp. 3571–3584, 2019.